Cellular/Molecular

Expression of Multiple P2X Receptors by Glossopharyngeal Neurons Projecting to Rat Carotid Body O_2-Chemoreceptors: Role in Nitric Oxide-Mediated Efferent Inhibition

Verónica A. Campanucci, Min Zhang, Cathy Vollmer, and Colin A. Nurse
Department of Biology, McMaster University, Hamilton, Ontario, Canada L8S 4K1

In mammals, ventilation is peripherally controlled by the carotid body (CB), which receives afferent innervation from the petrosal ganglion and efferent innervation from neurons located along the glossopharyngeal nerve (GPN). GPN neurons give rise to the "efferent inhibitory" pathway via a plexus of neuronal nitric oxide (NO) synthase-positive fibers, believed to be responsible for CB chemoreceptor inhibition via NO release. Although NO is elevated during natural CB stimulation by hypoxia, the underlying mechanisms are unclear. We hypothesized that ATP, released by rat CB chemoreceptors (type 1 cells) and/or red blood cells during hypoxia, may directly activate GPN neurons and contribute to NO-mediated inhibition. Using combined electrophysiological, molecular, and confocal immunofluorescence techniques, we detected the expression of multiple P2X receptors in GPN neurons. These receptors involve at least four different purinergic subunits: $P2X_2$ [and the splice variant $P2X_{2(b)}$], $P2X_3$, $P2X_4$, and $P2X_7$. Using a novel coculture preparation of CB type I cell clusters and GPN neurons, we tested the role of P2X signaling on CB function. In cocultures, fast application of ATP, or its synthetic analog 2′,3′-*O*-(4 benzoylbenzoyl)-ATP, caused type I cell hyperpolarization that was prevented in the presence of the NO scavenger 2-(4-carboxyphenyl)-4,4,5,5-tetramethyl-imidazoline-1-oxyl-3-oxide potassium. These data suggest that ATP released during hypoxic stress from CB chemoreceptors (and/or red blood cells) will cause GPN neuron depolarization mediated by multiple P2X receptors. Activation of this pathway will lead to calcium influx and efferent inhibition of CB chemoreceptors via NO synthesis and consequent release.

Key words: **ATP; CB chemoreceptors; efferent inhibition; glossopharyngeal neurons; hypoxia; NO; P2X receptor**

Introduction

The peripheral control of ventilation is mediated by chemoreceptors located in the carotid body (CB) which receives afferent innervation from the carotid sinus nerve (CSN), a branch of the glossopharyngeal nerve (Gonzalez et al., 1994). Thus, in response to a fall in blood partial pressure of oxygen (PO_2) (hypoxia), there is a compensatory reflex hyperventilation initiated by CB chemoreceptor cells, which release neurotransmitters, including ATP, that excite the CSN (Gonzalez et al., 1994; Nurse, 2005). In addition to this afferent pathway, there is a less well understood "efferent inhibitory" pathway that involves a plexus of neuronal nitric oxide synthase (nNOS)-positive nerve fibers that modulate CB function via release of NO (Prabhakar et al., 1993; Wang et al., 1993, 1995a,b; Grimes et al., 1994; Prabhakar, 1999). The origin of these nNOS-positive fibers includes two groups of autonomic neurons or "microganglia," one located near the branch point of the CSN and glossopharyngeal (GPN) nerve and the other located more distally along the GPN nerve (Wang et al., 1993, 1995a,b; Campanucci et al., 2003; Campanucci and Nurse, 2005). Although there is good evidence that the CB is a source of both nNOS and endothelial NO synthase isoforms and that NO has an inhibitory effect on CB function (Wang et al., 1995a,b; Kline et al., 1998; Prabhakar, 1999), the physiological role of each isoform during hypoxic chemoexcitation is not well understood. We are particularly interested in the nNOS isoform because it is expressed in neurons that contribute to the efferent inhibitory pathway to the CB. We reported recently (Campanucci et al., 2003; Campanucci and Nurse, 2005) that these nNOS-positive autonomic GPN neurons are hypoxia sensitive, and it is known that NO is released in the CB during hypoxia (Fung et al., 2001). However, the mechanisms leading to NOS activation, and consequent NO release, are unclear and confounded by the requirement of molecular oxygen for enzyme activity (Prabhakar, 1999).

In the present study, we considered ATP stimulation as a mechanism of activation of the CB efferent inhibitory pathway. ATP, released from CB chemoreceptors as a key excitatory neurotransmitter (Zhang et al., 2000; Rong et al., 2003; Buttigieg and Nurse, 2004; Nurse, 2005) and/or from circulatory red blood cells (Ellsworth, 2000) during hypoxia, may play a central role in the depolarization of GPN neurons, leading to NO synthesis and release. Autonomic neurons are known to express a variety of excitatory ionotropic purinergic P2X receptors, which act as

Received April 19, 2006; revised July 11, 2006; accepted Aug. 7, 2006.

This study was supported by Canadian Institutes for Health Research (CIHR) Grant MOP-57909 (C.A.N.). V.A.C. was supported by a scholarship from CIHR and a Dr. Sydney Segal research grant from The SIDS Foundation of Canada. We thank Stephen Brown for expert technical advice and unfailing assistance during the RT-PCR experiments, Dr. J. F. X. Jones for technical advice on Evans blue dye staining, and Dr. E. Cooper for his critical comments on this manuscript.

Correspondence should be addressed to Dr. Verónica A. Campanucci at her present address: Department of Physiology, McGill University, McIntyre Medical Science Building, Room 1129, 3655 Promenade Sir William Osler, Montréal, Québec, Canada H3G 1Y6. E-mail: veronica.campanucci@mcgill.ca.

DOI:10.1523/JNEUROSCI.1672-06.2006

 0270-6474/06/269482-12$15.00/0

ATP-gated nonselective cation channels with significant permeability to calcium (Ralevic and Burnstock, 1998; Dunn et al., 2001; North, 2002), whose cytosolic levels must reach the 400–1000 nM range to facilitate NOS activation (Vincent, 1994; Fung et al., 2001). Here we show that GPN neurons expressed at least four different types of P2X receptors ($P2X_2$, $P2X_3$, $P2X_4$, and $P2X_7$). Moreover, using a novel GPN–CB coculture system, we demonstrate that activation of P2X receptors in GPN neurons leads to NO-dependent inhibition of CB chemoreceptors (type I cells) after exposure to either ATP or hypoxia.

Materials and Methods

Cell culture. Wistar rat pups [9–12 d old; Harlan (Madison, WI) or Charles River (Québec, Québec, Canada)] were first stunned by a blow to the head that rendered them unconscious and then killed by decapitation. The carotid bifurcation, surrounding ganglia, and attached nerves were removed under sterile conditions. All procedures for animal handling were performed according to the guidelines of the Canadian Council on Animal Care. A section of the GPN, extending from its intersection with the CSN to a region ~5 mm distal to the intersection, was dissected bilaterally from each pup. Each GPN was then cut into two segments so as to separate the two populations (proximal and distal) of GPN neurons. The two segments were separately pooled, digested with enzyme [0.1% collagenase (Invitrogen, Burlington, Ontario, Canada), 0.1% trypsin, Sigma (St. Louis, MO), and 0.01% DNase (Invitrogen)] and mechanically dissociated to produce dispersed GPN neurons. The cell suspension was plated onto a thin layer of Matrigel (Collaborative Research, Bedford, MA) that was previously applied to the central wells of modified 35 mm tissue culture dishes. Cultures were grown at 37°C in a humidified atmosphere of 95% air–5% CO_2, and used for either patch-clamp experiments or immunofluorescence studies ~24–48 h after isolation. In some experiments, GPN neurons were cocultured with rat CB type I cells. To produce cocultures, an overlay of dissociated rat GPN neurons was added to a preexisting monolayer of CB type I cells prepared as described previously (Zhong et al., 1997; Nurse and Zhang, 1999; Zhang et al., 2000). Electrophysiological recordings from cocultures were usually performed ~3 d after the neurons were plated.

Organ culture. Whole mounts of the intact petrosal/glossopharyngeal nerve/carotid sinus nerve/CB complex were carefully dissected from rat pups (9–10 d old), taking care not to cut the CSN. In some cases, before organ culture, the petrosal ganglion was removed and the remaining tissue was placed on the membrane of Transwell-COL culture plates (Costar, Cambridge, MA). The preparation was semi-submerged and maintained in organ culture for 12–24 h at 35°C. After incubation, the whole mount was processed for immunofluorescence as described below.

Nystatin perforated-patch whole-cell recording. Nystatin perforated-patch, whole-cell recording was used in this study according to procedures described in detail previously (Zhong et al., 1997; Zhang et al., 2000). Patch pipettes were made from Corning 7052 glass (A-M Systems, Carlsborg, WA) or borosilicate glass (World Precision Instruments, Sarasota, FL) using a vertical puller (PP 83; Narishige, Tokyo, Japan) and were fire polished. Micropipettes had a resistance of 2–10 MΩ when filled with intracellular recording solution and formed gigaseals between 2 and 12 GΩ. In most experiments, ~75% of the series resistance was compensated, and junction potentials were cancelled at the beginning of the experiment. The extracellular fluid was warmed before entering the recording chamber, in which the mean temperature was 34 ± 2°C over the time course of the experiments. Whole-cell currents or membrane potentials were recorded with the aid of an Axopatch 1D amplifier (Molecular Devices, Palo Alto, CA) equipped with a 1 GΩ head-stage feedback resistor and a Digidata 1200 analog-to-digital converter (Molecular Devices) and stored on a personal computer. Current- and voltage-clamp protocols, data acquisition, and analysis were performed using pClamp software (version 6.0; Molecular Devices) and Axotape (version 2.02; Molecular Devices). ATP-induced currents were sampled at 0.5–1 kHz and stored on a computer for analysis with pClamp (version 9.0; Molecular Devices).

Solutions and drugs. Experiments were performed using extracellular fluid of the following composition (in mM): 110 NaCl, 5 KCl, 2 $CaCl_2$, 1 $MgCl_2$, 10 glucose, 12 sucrose, and 24 $NaHCO_3$, at pH ~7.4 (maintained by bubbling with 5% CO_2). For nystatin perforated-patch recordings (Zhong et al., 1997; Zhang et al., 2000), the pipette solution contained the following: 115 mM potassium glutamate or gluconate, 25 mM KCl, 5 mM NaCl, 1 mM $CaCl_2$, 10 mM HEPES, and 300 μg/ml nystatin, at pH 7.2. All solutions were filtered through a 0.2 μm Millipore (Bedford, MA) filter before use. During recordings, the culture was continuously perfused under gravity flow, and the fluid in the recording chamber was maintained at a constant level by suction. The following drugs were obtained from Sigma: tetrodotoxin; tetraethylammonium; ATP; α,β-methylene ATP (α,β-MeATP); 2′-3′-*O*-(4 benzoylbenzoyl)-ATP (BzATP); adenosine 5′-diphosphate-2′,3′-dialdehyde or oxidized-ATP (OxATP); ivermectin (IVM); brilliant blue G (BBG); 2-(4-carboxyphenyl)-4,4,5,5-tetramethyl-imidazoline-1-oxyl-3-oxide potassium (cPTIO); N_ω-nitro-L-arginine methyl ester hydrochloride (L-NAME); and sodium nitroprusside (SNP). All agonists (ATP, BzATP, and α,β-MeATP) were applied by a "fast perfusion" system using double-barreled pipettes, whereas modulators (i.e., IVM) and antagonists (suramin, OxATP, and BBG) were applied to the bath by perfusion under gravity (Zhong et al., 1997). EC_{50} and IC_{50} values were obtained by the best fit of the data using the Hill function. Results are represented as means ± SEM. Current densities (in picoamperes per picofarad) were compared using paired Student's *t* test. Membrane potentials before and after drug application were compared by repeated-measures ANOVA. Ratios were compared using a nonparametric test (Mann–Whitney). In all cases, the level of significance was set at $p < 0.05$.

Confocal immunofluorescence. Whole mounts of the freshly dissected GPN nerve or of organ culture explants (see above) were fixed in 4% paraformaldehyde overnight at 4°C. Cultures of dissociated GPN neurons were fixed for 15 min at room temperature (Campanucci et al., 2003). In experiments in which CB sections were immunostained, the animal was fixed by perfusion with PBS containing paraformaldehyde as described previously (Zhang et al., 2000). After washing in PBS (three times for 5 min), whole mounts were incubated for 72 h at 4°C with primary antibody; an overnight incubation was used for cultures. Primary antibodies used were as follows: polyclonal rabbit antibodies against rat $P2X_2$, $P2X_4$, and $P2X_7$ (1:200; Alomone Labs, Jerusalem, Israel), guinea pig anti-rat $P2X_3$ (1:500; Chemicon, Temecula, CA), polyclonal rabbit anti-rat nNOS (1:200; ImmunoStar, Hudson, WI), monoclonal mouse and polyclonal rabbit anti-rat tyrosine hydroxylase (TH) (1:1000; Chemicon), monoclonal mouse anti-rat neurofilament (NF) (68 kDa; 1:5; Boehringer Mannheim, Montreal, Quebec, Canada), and monoclonal mouse anti-rat GAP-43 (1:20,000). The primary antiserum was diluted in PBS containing 1% BSA and 0.5% Triton X-100. After incubation, the samples were washed in PBS (three times for 5 min) and incubated in the dark for 1 h at room temperature with the secondary antibody conjugated to Alexa 594 (1:500; Invitrogen), Texas red (1:50; Jackson ImmunoResearch, West Grove, PA) or FITC (1:50; Cappel, Malvern, PA). The secondary antiserum was diluted in PBS containing 1% BSA and 0.5% Triton X-100. Samples were covered with a photobleaching reagent (Vectashield; Vector Laboratories, Burlingame, CA) and viewed with a confocal microscope (Microradiance 2000; Bio-Rad, Mississauga, Ontario, Canada) equipped with argon (two lines, 488 and 514 nm) and helium/neon (543 nm) lasers. Tissue was scanned in optical sections separated by 1–2 μm at a rate of 166 lines per second, and scanning was controlled with the aid of Lasersharp software. Between 10 and 30 μm of tissue in each whole-mount preparation was routinely scanned in this manner. In control experiments, either preincubation with blocking peptide or omission of the primary antibody resulted in complete abolition of staining. Blocking peptides for $P2X_2$, $P2X_4$, $P2X_7$ (Alomone Labs), and $P2X_3$ (Chemicon) were preincubated with primary antibody (3 μg peptide/3 μg antibody) overnight at 4°C before application. Image processing and manipulation was performed using CorelDraw 9 (Corel, Ottawa, Ontario, Canada).

Reverse transcriptase-PCR. Total RNA was extracted from ~18 short (2–3 mm) segments of the glossopharyngeal nerve containing the distal population of GPN neurons using Bio-Rad AURUM TOTAL RNA Mini

kit. RNA was reverse transcribed using Bio-Rad iScript cDNA Synthesis kit or Superscript III, RNase H-Reverse Transcriptase (Invitrogen). Gene-specific primers were designed using GeneFisher (Giegerich et al., 1996) and synthesized by The Central Facility of the Institute for Molecular Biology and Biotechnology (MOBIX) (McMaster University, Hamilton, Ontario, Canada). The following primers were used and are listed as sequence amplified, 5′ to 3′ upstream primer sequence, 5′ to 3′ downstream primer sequence, and size of product(s): glyceraldehyde-3-phosphate dehydrogenase (GAPDH), 5′ TTC ACC ACC ATG GAG AAG GC 3′, 5′ GGC ATG GAC TGT GGT CAT GA 3′, 230 bp; $P2X_2$/$P2X_{2(b)}$, 5′AAG TTG GGC CAA ACC TTT G 3′, 5′ ACC CCA AAT ATT CTT TCC GG 3′, 600 and 400 bp; $P2X_3$, 5′ TTG AGG GTA GGG GAT GTG GT 3′, 5′ GCT GAT AAT GGT GGG GAT GA 3′, 326 bp; $P2X_4$, 5′ AGT CTG TGA AGA CCT GTG A 3′, 5′ GGA GAC ACA TTH TGT TCC A 3′, 408 bp; and $P2X_7$, 5′ AGA CAA ACA AAG TCA CCC GG 3′, 5′ GGT ATA CAC CTG CCG GTC TGG 3′, 400 bp.

DNA was amplified in a single round of PCR using either *Taq*DNA Polymerase High Fidelity (Invitrogen) or SuperTaq Polymerase (Ambion, Austin, TX).

PCR was held at 94°C for 2 min and cycled 35 times. Each cycle consisted of 94°C for 30 s (denaturation), 52°C [$P2X_2$ and $P2X_{2(b)}$], 55°C ($P2X_3$ and GAPDH), 58°C ($P2X_7$), and 50°C ($P2X_4$) for 30 s (annealing), and 72°C for 1 min (extension). This was followed by a 10 min final extension at 72°C. PCR products were visualized on an ethidium bromide-stained 2% agarose gel under ultraviolet illumination. The 1 kb plus ladder used was obtained from Invitrogen. The QIAquick Gel Extraction kit (Qiagen, Mississauga, Ontario, Canada) was used to extract PCR fragments from the agarose gel. The DNA sample was then sequenced (at MOBIX) using an ABI Prism automated Sequencer (with T7 polymerase). The sequencing results were analyzed by BLAST2 (basic local alignment search tool), an NIH computer software for identification of gene sequences. The sequences were matched to the *Rattus norvegicus* $P2X_2$ (GenBank accession number NM_053656), $P2X_{2(b)}$ splice variant (GenBank accession number Y10473), $P2X_3$ (GenBank accession number X91167), $P2X_4$ (GenBank accession number X93565), and $P2X_7$ (GenBank accession number X95882.1).

Paraganglia staining. Rat pups (10–14 d old) were anesthetized by intraperitoneal administration of Somnotol (65 mg/kg), before perfusion via the aorta with PBS, followed by PBS containing 4% paraformaldehyde. Fixed animals were then perfused with filtered (0.2 μm Millipore filter) Evans blue dye (100 mg of dye per milliliter of 0.9% NaCl, adjusted pH to 7.4), so as to stain paraganglia attributable to the high permeability of their blood vessels to large dye molecules (McDonald and Blewett, 1981). The carotid bifurcation was then excised, and the tissue was mounted in fresh PBS. Images were captured with a Zeiss (Oberkochen, Germany) S16 upright microscope equipped with a Retiga monochrome 12-bit digital camera (QImaging, Burnaby, British Columbia, Canada), with the aid of Northern Eclipse software (Empix Imaging, Mississauga, Ontario, Canada).

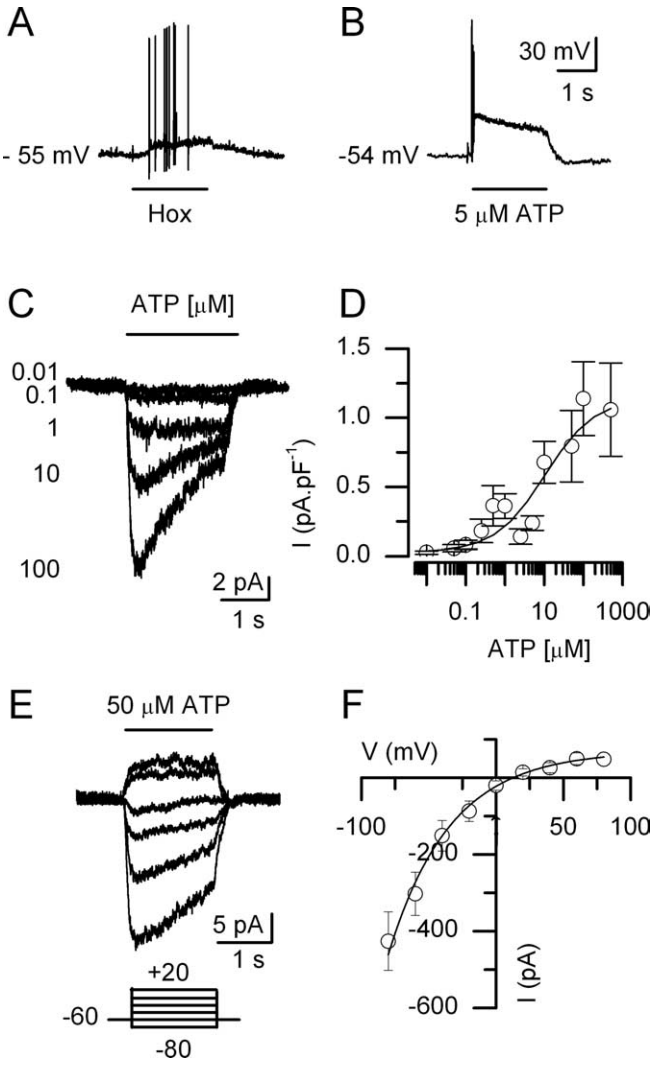

Figure 1. ATP-evoked responses in O_2-sensitive GPN neurons. ***A***, ***B***, Representative traces showing the effects of hypoxia (Hox) and ATP, respectively, on membrane potential of the same distal GPN neuron 24 h after isolation. Traces obtained during current-clamp recording. ***C***, Voltage-clamp current recordings of ATP-evoked inward currents at −60 mV attributable to increasing concentrations of ATP applied to a distal GPN neuron. ***D***, Dose–response curve for ATP is shown on the right for a group of 11 GPN neurons (apparent EC_{50} of 10.5 μM). ***E***, Traces of ATP-evoked current in a GPN neuron at different membrane potentials. ***F***, *I–V* plot of ATP-evoked current for a group of seven neurons; note inward rectification and reversal potential at ~0 mV.

Results

ATP-evoked responses in GPN neurons

As described previously (Campanucci et al., 2003), GPN neurons are concentrated in two groups, one proximal and near the CSN bifurcation and the other located more distally along the GPN. Before ATP application, GPN neurons from both groups were tested for O_2 sensitivity by perfusing the culture with a hypoxic solution (PO_2 of ~15 Torr) as described previously (Campanucci et al., 2003). Essentially all neurons (>90%) responded to hypoxia with membrane depolarization that was sometimes large enough to trigger action potentials (Fig. 1*A*). Rapid perfusion of ATP (5 μM) over such neurons caused membrane depolarization and action potential firing (Fig. 1*B*). Under voltage clamp at −60 mV, ATP evoked a dose-dependent inward current in GPN neurons with an apparent EC_{50} of ~10.5 μM ($n = 11$) (Fig. 1*C*,*D*). These data were not well fitted by a simple Hill equation, suggesting that multiple receptors were involved. The reversal potential of the ATP-evoked current occurred near 0 mV ($n = 7$) (Fig. 1*E*,*F*), suggesting that it was carried by nonselective cation channels. In addition, the ATP-evoked current showed typical inward rectification (Fig. 1*F*), as described previously for currents carried by P2X purinergic receptors (Brake et al., 1994; Evans et al., 1996) (for review, see North, 2002).

Evidence for functional expression of $P2X_2$–$P2X_3$ heteromeric receptors

The kinetic profile of ATP-evoked inward currents in GPN neurons indicated a fast activation phase, followed by slow inactivation (Fig. 1*C*, see example traces). Such biphasic kinetics are characteristic of cells expressing $P2X_2$ and $P2X_3$ homomeric or $P2X_2$–$P2X_3$ heteromeric receptors (North, 2002). Consistent with the presence of $P2X_2$–$P2X_3$ heteromeric receptors (Radford et al., 1997), α,β-MeATP evoked slowly desensitizing inward

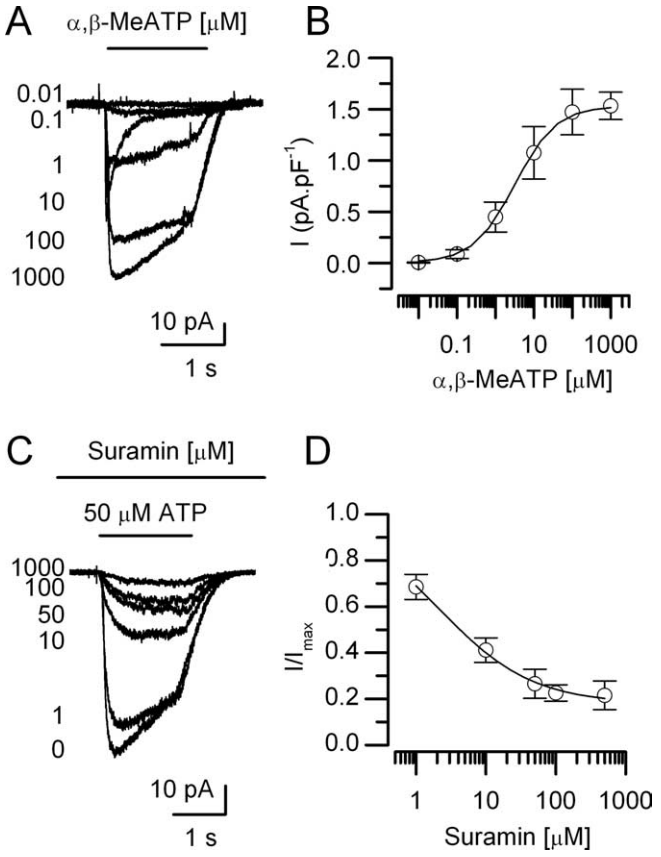

Figure 2. Effects of ATP agonists and antagonists on GPN neurons. ***A***, Current traces show a representative example of α,β-MeATP-evoked currents at −60 mV attributable to increasing concentrations of the agonist on a distal GPN neuron. ***B***, Dose–response curve for α,β-MeATP is shown for a group of five distal neurons (EC_{50} of 3.2 μM). ***C***, Current traces evoked by application of 50 μM ATP in the presence of increasing doses (values on left, in micromolar) of the nonselective purinergic receptor antagonist suramin. ***D***, Dose–response curve of the inhibitory effect of suramin on the ATP-evoked response in a group of five distal GPN neurons. Note that even high doses of suramin were insufficient to block completely the currents evoked by 50 μM ATP.

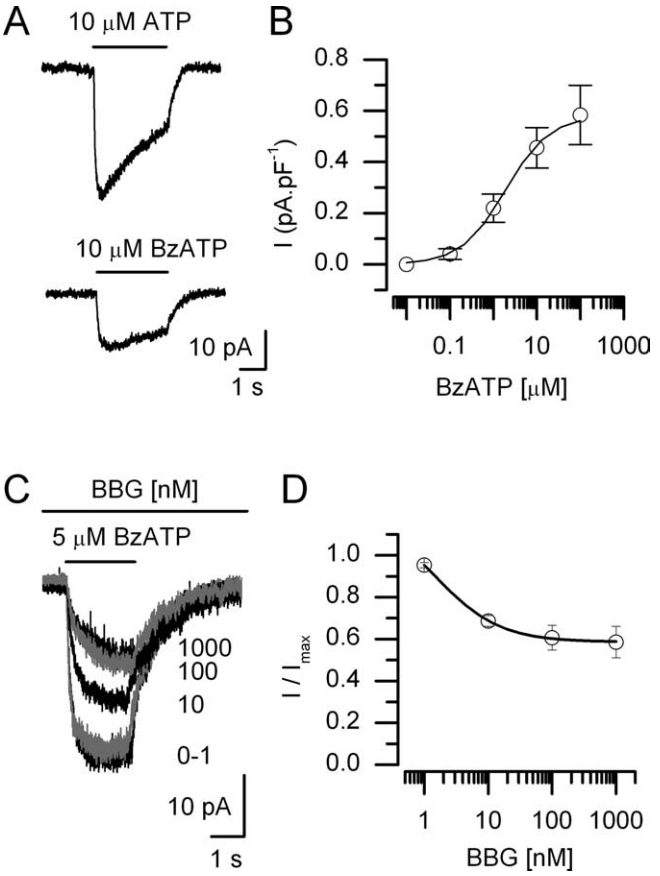

Figure 3. Effects of $P2X_7$ agonists and antagonists on GPN neurons. ***A***, Representative current traces elicited by application of ATP (10 μM) and the high-potency $P2X_7$ agonist BzATP (10 μM) at −60 mV on a distal GPN neuron. ***B***, Dose–response curve for BzATP is shown for a group of four distal GPN neurons (EC_{50} of 1.9 μM). ***C***, Example current traces showing the effects of the $P2X_7$ receptor blocker BBG on BzATP-evoked currents; concentrations of BBG are shown to the right of traces. ***D***, Dose–response curve for BBG inhibition of BzATP-evoked currents ($n = 5$). Note that BBG at nanomolar concentrations blocked a component of the BzATP-evoked current, suggesting the functional expression of $P2X_7$ homomeric receptors in GPN neurons.

currents (at −60 mV) with an EC_{50} of ~3.2 μM (Fig. 2*A*,*B*). These data suggest that GPN neurons express $P2X_2$–$P2X_3$ heteromeric receptors, although the expression of $P2X_2$ and $P2X_3$ homomeric forms cannot be excluded.

In addition, our experiments with the nonselective purinergic antagonist suramin (North and Surprenant, 2000) indicated that multiple P2X receptors are expressed in a single GPN neuron. During application of 50 μM ATP in the presence of high doses of suramin (500–1000 μM), concentrations expected to block $P2X_2$ and $P2X_3$ homomeric and heteromeric receptors (North and Surprenant, 2000), we observed a residual inward current (Fig. 2*C*,*D*), whose amplitude was ~20% of the total ATP-evoked inward current (Fig. 2*D*). These findings suggest that, in addition to contributions from $P2X_2$ and $P2X_3$ subunits, other P2X purinergic subunits are involved.

Evidence for functional expression of $P2X_7$ homomeric receptors

Both $P2X_7$ and $P2X_4$ display low sensitivity to suramin when heterologously expressed in their homomeric forms (Ralevic and Burnstock, 1998; North and Surprenant, 2000; Khakh, 2001; Khakh et al., 2001). Therefore, either of these two subtypes could be present in GPN neurons. To test for functional expression of $P2X_7$ receptors, we applied low micromolar concentrations of BzATP, an agonist with even greater potency for $P2X_7$ receptors than ATP (North and Surprenant, 2000; North, 2002). BzATP had an EC_{50} of ~1.9 μM ($n = 4$) (Fig. 3*B*). These data suggest that at least a population of purinergic receptors expressed in GPN neurons has moderate-to-high affinity for BzATP, and this is consistent with the expression of homomeric $P2X_7$ receptors (North, 2002).

Because micromolar concentrations of BzATP also activate heterologously expressed rat $P2X_1$, $P2X_2$, and $P2X_3$ homomeric, as well as rat $P2X_2$–$P2X_3$ heteromeric, receptors (Bianchi et al., 1999; North and Surprenant, 2000), it was necessary to confirm the presence of $P2X_7$ receptors by other methods. We therefore used the antagonist BBG (0.1–100 nM) (Fig. 3*C*), which is reported to be a selective blocker of heterologously expressed rat $P2X_7$ receptors in the nanomolar concentration range (Jiang et al., 2000). BBG at concentrations between 10 and 100 nM inhibited up to ~40% of the BzATP-evoked inward current ($n = 5$) (Fig. 3*D*) in GPN neurons. Moreover, additional confirmation of the functional expression of $P2X_7$ receptors was obtained after exposure to the irreversible $P2X_7$-selective antagonist OxATP (Murgia et al., 1993). In these experiments, we first preincubated GPN neurons with 300 μM OxATP for 2 h at 37°C to block $P2X_7$ receptors (Murgia et al., 1993) and then tested the sensitivity of

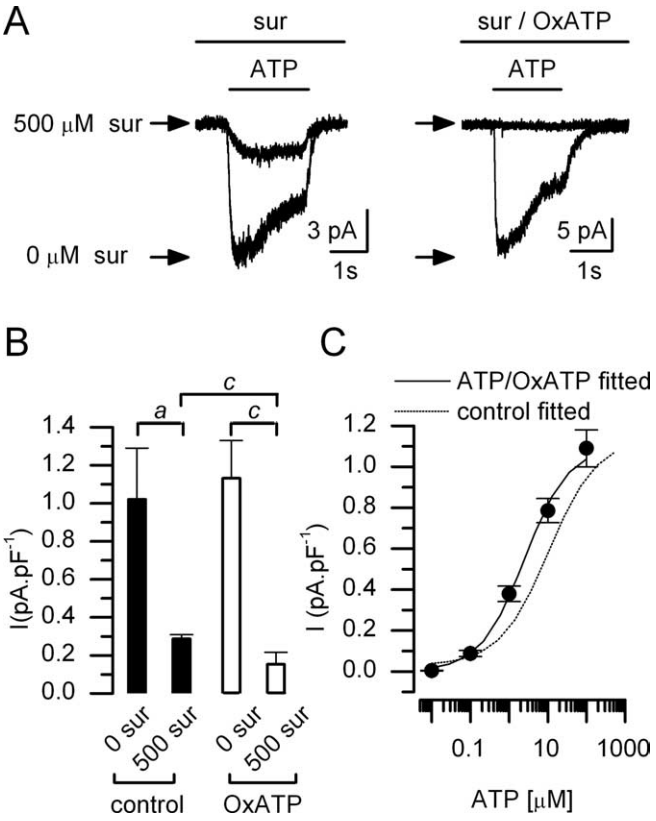

Figure 4. Effect of pretreatment with OxATP on the suramin sensitivity of the ATP-evoked response in GPN neurons. ***A***, Example traces showing the effects of 0 and 500 μM suramin (sur) on the ATP-evoked (50 μM) currents from cells under two different conditions, control (left traces) and after preincubation with the irreversible $P2X_7$-selective blocker OxATP at 500 μM (2 h at 37°C; right traces). Note that, after preincubation with OxATP, suramin (500 μM) abolished the ATP-evoked response in this cell. ***B***, Histogram comparing the ATP-evoked current density (in picoamperes per picofarad) with and without 500 μM suramin. Data are presented as mean ± SEM; black bars represent control (without OxATP; $n = 5$), and white bars represent cells pretreated with OxATP ($n = 11$). $^a p < 0.05$; $^c p < 0.001$. ***C***, Dose–response curve for ATP is shown for cells preincubated with OxATP. Data obtained from OxATP pretreated cells (solid line) are compared with those from control untreated cells (dotted line); note the significant reduction in EC_{50} for the OxATP-treated group (EC_{50} of ~2.5 μM) relative to control (EC_{50} of ~10.5 μM; $p < 0.05$; $n = 5$).

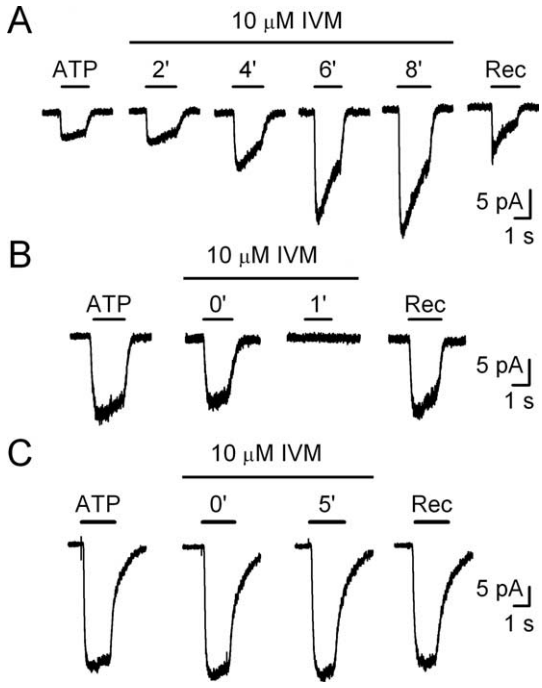

Figure 5. Effects of IVM on the ATP-evoked current in GPN neurons. ***A***, IVM (10 μM) caused potentiation of the currents evoked by 2 μM ATP; this occurred in 5 of 13 cells tested. These data provide functional evidence for the expression of $P2X_4$ purinergic receptors in GPN neurons. In addition, IVM caused inhibition of the ATP-evoked response in 5 of 13 cells (as exemplified in ***B***) and had no effect in the remaining cases (***C***).

the remaining ATP-evoked currents to suramin. Pretreatment with OxATP decreased the residual ATP-evoked current observed in the presence of high doses of suramin (Fig. 4*A*,*B*), such that the residual current significantly decreased from 0.31 ± 0.02 pA/pF ($n = 11$) in control cells to 0.15 ± 0.06 pA/pF ($n = 5$) in cells pretreated with OxATP ($p < 0.001$). Moreover, the half-maximal ATP concentration (EC_{50}) for OxATP-pretreated cells was ~2.5 μM, a value significantly lower than that for control cells (EC_{50} of ~10.5 μM; $p < 0.05$), consistent with inhibition of $P2X_7$ receptors. This is illustrated by the leftward shift of the dose–response relationship for cells pretreated with OxATP (Fig. 4*C*). Together, these data provide evidence for the functional expression of $P2X_7$ receptors in GPN neurons and further imply that, when these receptors are chemically disabled, purinergic signaling is maintained at least in part by purinoceptors containing $P2X_2$ and $P2X_3$ subunits.

Functional evidence for the expression of $P2X_4$ receptors in GPN neurons

In approximately one in three neurons that were preincubated with OxATP, a substantial ATP-evoked current persisted in the presence of high doses (500–1000 μM) of suramin (data not shown), suggesting the presence of other P2X receptor subtype(s) distinct from $P2X_7$. One candidate, homomeric $P2X_4$ receptors, is known for its relative insensitivity to suramin (North and Surprenant, 2000). To test whether GPN neurons also expressed functional $P2X_4$ receptors, we used IVM, a channel modulator that has been shown to enhance specifically $P2X_4$-mediated currents in heterologous expression systems (Khakh et al., 1999). IVM (2–10 μM) caused potentiation of the ATP-evoked current in 5 of 13 GPN neurons tested (Fig. 5*A*). For reasons that are not presently understood, this drug also had an inhibitory effect in 5 of 13 (Fig. 5*B*) of neurons tested. Last, IVM had no effect in 3 of 13 neurons tested, suggesting the lack of expression of functional $P2X_4$ receptors (Fig. 5*C*).

Expression of P2X subunits in glossopharyngeal nerve using reverse transcriptase-PCR techniques

To corroborate the expression pattern of P2X receptors as revealed by immunofluorescence (see below) and electrophysiological studies, short segments of glossopharyngeal nerve containing the distal population of GPN neurons were analyzed by reverse transcriptase (RT)-PCR techniques using appropriate primers (see Materials and Methods). As illustrated in Figure 6, bands of the expected size indicated mRNA expression of $P2X_2$ (or $P2X_{2a}$), $P2X_{2(b)}$ splice variant, $P2X_3$, $P2X_4$, and $P2X_7$. Sequence analysis confirmed that the amplified products were identical (95–98%) to the known sequences for each subunit (supplementary data, available at www.jneurosci.org as supplemental material).

Cellular localization of $P2X_2$, $P2X_3$, $P2X_7$, and $P2X_4$ subunits *in situ*

Results from the functional, pharmacological, and expression studies discussed above led us to investigate the localization of

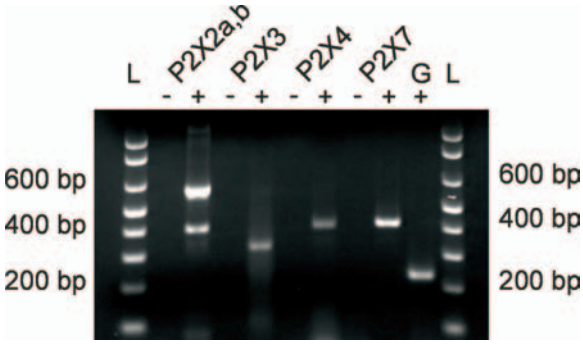

Figure 6. Detection of mRNA for $P2X_2$, $P2X_3$, $P2X_4$, and $P2X_7$ in excised tissue samples containing distal GPN neurons. RT-PCR was performed on these samples using gene-specific primers for $P2X_2/P2X_{2(b)}$ (designated P2X2a,b), $P2X_3$, $P2X_4$, and $P2X_7$ subunits and the housekeeping gene GAPDH (G). Expected product sizes are as follows: $P2X_2/P2X_{2(b)}$, 600 and 400 bp; $P2X_3$, 326 bp; $P2X_4$, 408 bp; $P2X_7$, 400; and GAPDH, 230 bp. The ladder lane (L) shows bands at 100 bp increments. In negative control reactions without RT (−), no PCR products were observed. PCR products were identified with 2% agarose gel stained with ethidium bromide and viewed under UV illumination.

$P2X_2$, $P2X_3$, $P2X_4$, and $P2X_7$ subunits in freshly dissected whole mounts of GPN nerve using immunofluorescence. As described previously (Campanucci et al., 2003), these neurons are concentrated in two groups, one proximal and near the CSN bifurcation and the other located more distally along the GPN. For both proximal (Fig. 7*A–C*) and distal (Fig. 7*D–F*) populations, there was colocalization of $P2X_2$ and $P2X_3$ subunits in the soma of GPN neurons as revealed by double-labeled immunofluorescence ($n = 10$). These data are consistent with the functional evidence for heteromeric $P2X_2$–$P2X_3$ receptors.

Because our electrophysiological data suggested the presence of $P2X_4$ receptors in at least a subpopulation of GPN neurons, we used immunofluorescence to localize $P2X_4$ subunits. Consistent with the data reported above, positive $P2X_4$ immunofluorescence was localized in both populations of GPN neurons (Fig. 7*G–L*). However, the majority of NF/GAP-43-positive neurons observed along the GPN expressed immunoreactive $P2X_4$ subunits ($n = 10$) (Fig. 7*G–I*). This contrasts with our electrophysiological data, which suggested that only ~38% of GPN neurons expressed functional homomeric $P2X_4$ receptors. In addition, $P2X_4$ immunofluorescence colocalized with that of $P2X_3$ in GPN cell bodies ($n = 5$) (Fig. 7*J–L*). These data confirm the expression of multiple P2X receptors in the same GPN neuron.

The distribution of $P2X_7$ immunostaining was more complex. Whereas $P2X_7$ subunits were localized in NF-positive cell bodies of the proximal GPN neurons ($n = 7$) (Fig. 8*A–C*), on the distal population, they appeared targeted to nerve endings surrounding the NF-positive cell bodies ($n = 7$) (Fig. 8*D–F*). Because both neuronal populations project to the CB (Wang et al., 1993, 1994; Campanucci et al., 2003), we also investigated the distribution of $P2X_7$ immunoreactivity in tissue sections of the CB. We identified nerve terminals immunoreactive to NF and GAP-43 ($n = 5$) (Fig. 8*G*) in the CB; $P2X_7$ punctate immunoreactivity colocalized with these nerve terminals in defined regions of the CB (Fig. 8*H*, *I*, arrows). Interestingly, punctate $P2X_7$ immunostaining was seen near TH-positive clusters of CB chemoreceptor cells as illustrated in Figure 8*J* ($n = 3$). Furthermore, in CB cryosections, $P2X_7$ immunoreactivity colocalized with that of $P2X_3$ in nerve endings surrounding chemoreceptor cell clusters (data not shown), suggesting that GPN nerve terminals may also express multiple P2X receptor subunits, similar to the soma.

The CB receives both afferent innervation from the petrosal ganglion and efferent innervation from the GPN. Therefore, to determine whether this $P2X_7$ immunostaining in the CB was solely of GPN origin, we performed "denervation" experiments. The small size of the GPN makes this extremely difficult *in vivo*, so we performed these experiments by transplanting the intact GPN, CSN, and CB to organ culture (incubated for 12 h at 37°C); in doing so, we effectively axotomized the afferent axons whose cell bodies are located in the petrosal ganglion. In these experiments, we observed a dramatic reduction in NF and GAP-43 staining of axons projecting to the CB. However, there were no significant differences in $P2X_7$ puncta near clusters of CB chemoreceptor cells ($n = 5$; data not shown), suggesting that the GPN was at least a major source of $P2X_7$ innervation in the CB. Equally important in these preparations, we observed several nNOS-positive nerve processes in close proximity to TH-positive CB chemoreceptor clusters (Fig. 8*K*), consistent with the proposal that local interactions may occur between GPN processes and CB chemoreceptor cells *in situ* (see below).

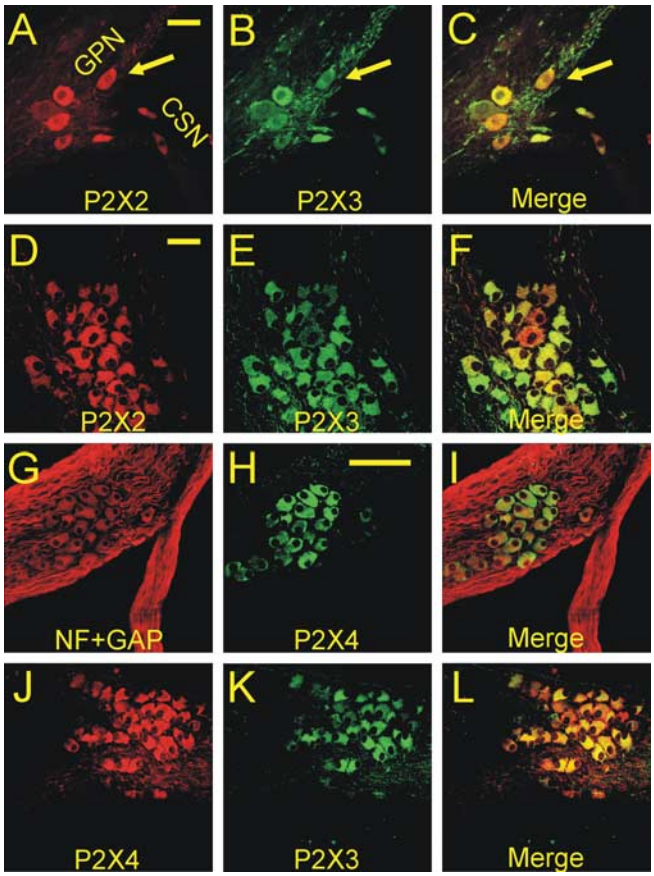

Figure 7. Localization of purinergic subunits in GPN neurons *in situ* by confocal immunofluorescence. Proximal neurons located at the bifurcation of the GPN and CSN expressed both $P2X_2$ (***A***; red) and $P2X_3$ (***B***; green) immunofluorescence; note colocalization in merged images. ***C***, Similarly, many neurons at the distal bifurcation coexpressed $P2X_2$ and $P2X_3$ subunits (***D–F***). ***G–I*** show colocalization of $P2X_4$ purinergic subunit (green) with the neuronal marker NF (red) in proximal GPN neurons. In ***J–L***, there is colocalization of $P2X_4$ (red) and $P2X_3$ (green) subunits in the distal population of GPN neurons. Scale bars: ***A–F***, 50 μm; ***G–L***, 100 μm.

Localization of $P2X_7$ immunofluorescence in cultured GPN neurons

Our immunocytochemical studies *in situ* indicated that $P2X_7$ receptors are localized to nerve terminals rather than on the soma of the distal population (Fig. 8*D–F*); however, our electrophysi-

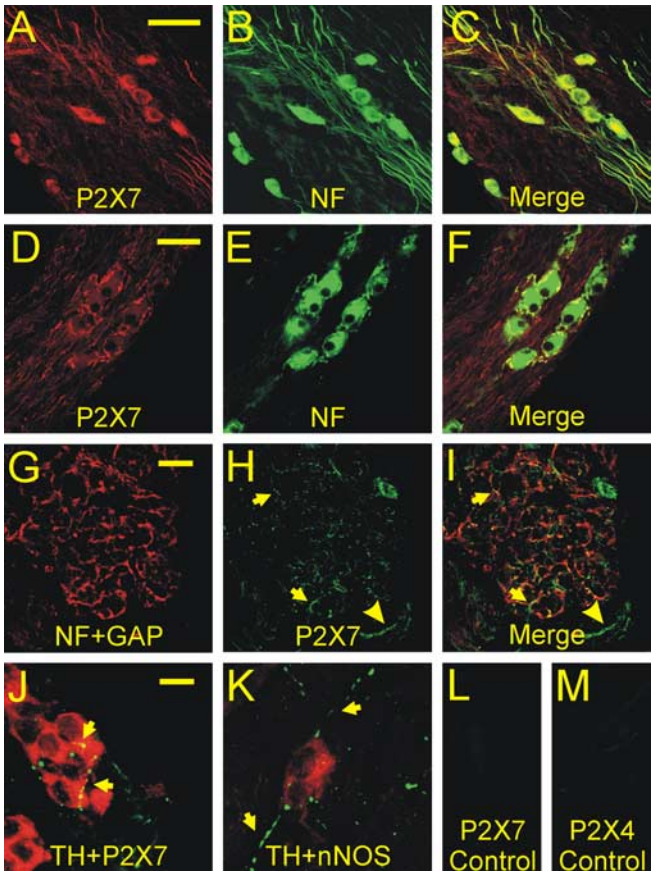

Figure 8. Immunolocalization of P2X subunits in GPN neurons and in nerve processes adjacent to CB chemoreceptors *in situ*. ***A–C***, Colocalization of $P2X_7$ purinergic subunit (red) with the neuronal marker NF (green) in proximal GPN neurons. In contrast, in ***D–F***, the distal GPN neurons failed to express $P2X_7$ subunits in their NF-positive soma (***K***) but were surrounded by $P2X_7$-positive nerve endings (***D–F***). ***G–I***, Colocalization of $P2X_7$ (green) and neuronal markers (NF + GAP; red) on nerve endings in tissue sections of rat CB. Nerve processes surround CB type I cell clusters that are not labeled in this section; arrows in ***H*** and ***I*** show regions of colocalization. Note that the $P2X_7$ labeling at bottom right in ***H*** and ***I*** was not associated with nerve endings (arrowhead). ***J***, Localization of TH and $P2X_7$ immunoreactivity in CB tissue section; note that punctuate $P2X_7$ immunostaining (green) is closely associated with a TH-positive (red) type I cell cluster. ***K***, Localization of nNOS and $P2X_7$ immunoreactivity in CB tissue section. Note the close association of punctate nNOS-immunoreactive processes (green) with TH-positive (red) type I cells. In control experiments, preincubation with blocking peptides for $P2X_7$ and $P2X_4$ antibodies abolished all immunostaining in ***L*** and ***M***, respectively. Scale bars: ***A–C***, ***G–I***, 50 μm; ***D–F***, 100 μm; ***J***, ***K***, 10 μm.

ological results on freshly isolated neurons (≤24 h in culture) showed that both populations of GPN neurons expressed functional $P2X_7$ receptors on their cell bodies. Our explanation for these results is that $P2X_7$ receptors undergo a redistribution when neurons are isolated in culture and now target to the soma. To examine whether $P2X_7$ undergo a redistribution, we immunolocalized $P2X_7$ subunits in freshly-isolated GPN neurons (≤24 h old, i.e., conditions used for patch-clamp experiments) and on GPN neurons in culture for 48–72 h. Interestingly, in freshly isolated neurons, $P2X_7$ immunofluorescence was concentrated on the cell bodies of both populations of GPN neurons ($n = 10$) (Fig. 9*A–C*). However, at 48–72 h after isolation, the $P2X_7$ immunostaining was weaker in the cell bodies and was detected along nerve processes ($n = 5$) (Fig. 9*D–F*). These data suggest that, shortly after axotomy *in vitro*, $P2X_7$ subunits undergo a redistribution and target to the soma of GPN neurons and that, over time in culture, the receptors are targeted, or transported away from the soma, to the nerve processes.

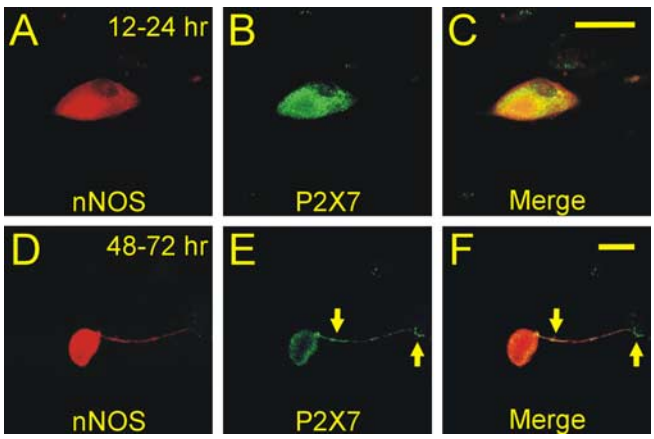

Figure 9. Confocal immunolocalization of nNOS and $P2X_7$ subunits in cultured GPN neurons from the distal population. ***A–C***, Colocalization of nNOS and $P2X_7$ immunoreactivity in same neuronal cell body ~24 h after isolation (i.e., approximate culture duration for patch-clamp experiments). ***D–F***, Similar experiment as in ***A–C***, except that immunostaining was done 48–72 h after cell isolation. Note that, at this time, $P2X_7$ immunoreactivity was less concentrated in cell bodies and was detected along neuronal processes and their endings. Scale bars, 30 μm.

Effects of P2X receptor stimulation and hypoxia on NO signaling in cocultures of GPN neurons and carotid body chemoreceptors

During hypoxia, ATP is released from CB chemoreceptors (Zhang et al., 2000; Rong et al., 2003; Buttigieg and Nurse, 2004; Nurse, 2005) and/or from circulatory red blood cells (Ellsworth, 2000), suggesting that it may play a central role in the depolarization of GPN neurons, leading to activation of the CB efferent inhibitory pathway via release of NO (Wang et al., 1993, 1995a;b; Prabhakar, 1999). We hypothesized that stimulation of P2X receptors on GPN neurons leads to NOS activation and NO synthesis and release, which will cause hyperpolarization of CB chemoreceptors. To test this idea, we developed a novel coculture preparation of GPN neurons and CB receptor (type I) cell clusters. Thus, an overlay of dissociated rat GPN neurons was added to a preexisting monolayer of cultured CB type I cells, which lack P2X receptors at least at the ages (9–10 d) used in these studies (Zhang et al., 2000; Prasad et al., 2001) (but see Xu et al., 2005; He et al., 2006). GPN neurons, "juxtaposed" (JGPN) to type I cell clusters in coculture (Fig. 10*A–C*), were selected for rapid application of either ATP (5–10 μM) or BzATP (5 μM) while membrane potential was simultaneously monitored in a type I cell within the adjacent cluster. As reported previously (Zhang et al., 2000), 10–100 μM ATP had negligible effects on the resting potential of clustered type I cells cultured without neurons (mean ΔV_m was 0.3 ± 0.1 mV; $n = 30$; $p > 0.05$) (Fig. 10*D*), and this was also the case for the $P2X_7$ receptor agonist BzATP ($n = 4$) (Fig. 10*E*). However, in a few cases ($n = 5$; data not shown), ATP caused a small hyperpolarization (1.4 ± 0.5 mV; $p < 0.05$) (Xu et al., 2005).

Interestingly, application of BzATP (5 μM) to JGPN neurons in coculture caused a strong hyperpolarization (~8 mV) of CB type I cells within the adjacent cluster (Fig. 10*G*); the membrane potential hyperpolarized from a mean resting level of −44.7 ± 3.1 to −52.2 ± 3.3 mV ($n = 8$) during BzATP application. In two cases from similar cocultures (Fig. 10*F*), BzATP also caused inhibition of the spontaneous activity that is sometimes seen in type I cells within large clusters (Zhang and Nurse, 2000). Because BzATP tended to produce irreversible long-term changes in type I cell membrane potential observed at ≥30 min after original

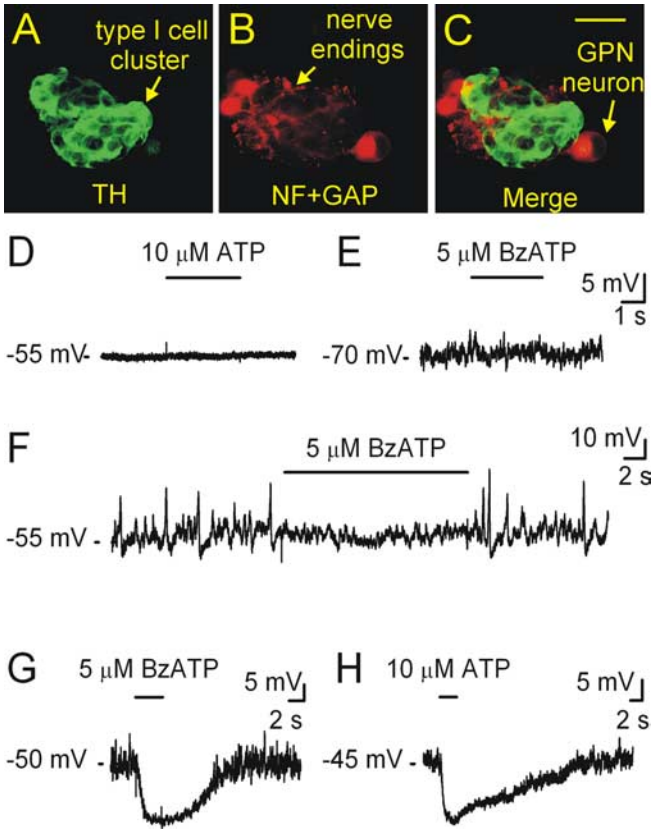

Figure 10. Effects of ATP and BzATP on the membrane potential of type I cells cultured with and without JGPN neurons. ***A–C***, Confocal immunofluorescence of coculture showing a cluster of TH-positive type I cells (green) in intimate association with several JGPN neurons and their processes that were immunopositive for NF and GAP-43 (red). Scale bar, 50 μm. ***D***, ***E***, Lack of effect of ATP (10 μM) and BzATP (5 μM) applied by rapid perfusion during the period indicated by the top horizontal bars on the membrane potential of type I cells cultured alone. In ***F–H***, recordings were obtained from type I cells in close proximity to JGPN neurons (***A–C***), which therefore could be directly stimulated during application of the P2X agonist. In ***F***, application of BzATP caused inhibition of spontaneous activity in a type I cell, whereas in ***G*** and ***H***, there was a marked type I cell hyperpolarization during application of BzATP and ATP, respectively.

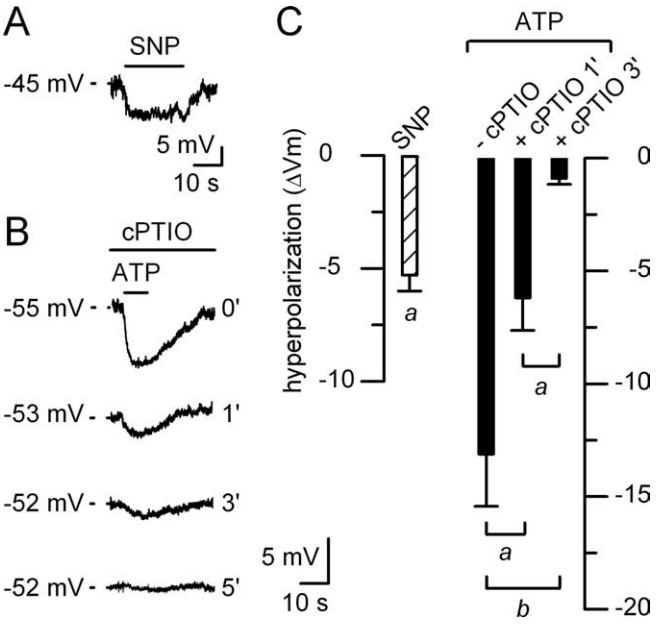

Figure 11. Effect of the NO donor sodium nitroprusside on the resting potential of type I cells and the NO scavenger cPTIO on the ATP-induced hyperpolarization in type I cells cocultured with GPN neurons. In ***A***, exposure of type I cell cultures (grown in the absence of GPN neurons) to SNP (500 μM) caused a reversible hyperpolarization of a type I cell membrane potential. In ***B***, a 5 min incubation of the coculture with the NO scavenger cPTIO (500 μM) caused a gradual reduction of the ATP-induced hyperpolarization in a type I cell, presumably mediated indirectly via NO release from activated adjacent JGPN neurons. ***C***, Hatched bar on left shows the mean amplitude of type I cell hyperpolarization (ΔV_m) caused by SNP ($n = 9$) in CB cultures grown without neurons; initial resting potential was -47.3 ± 4.8 mV. Filled bars on right compare time-dependent changes in magnitude of the ATP-induced hyperpolarization (ΔV_m) in a group of cocultured type I cells ($n = 6$) when exposed to cPTIO for 0, 1, and 3 min as in ***B***. Data are presented as mean ± SEM. $^a p < 0.05$; $^b p < 0.001$.

BzATP application, we tested the effects of the naturally occurring nucleotide ATP, which is itself released from CB type I cells during hypoxia (Zhang et al., 2000; Buttigieg and Nurse, 2004; Zhang and Nurse, 2004). Moreover, type I cells *in situ* are seen in close proximity to $P2X_7$- and nNOS-positive terminals of GPN neurons (Fig. 8*J*,*K*). As shown in Figure 10*H*, ATP also caused a strong hyperpolarization (~10 mV; $n = 7$) in cocultured type I cells without producing any long-term changes in membrane potential; the latter hyperpolarized from a mean resting level of -44.6 ± 3.0 to -54.5 ± 3.3 mV ($n = 7$) in the presence of ATP.

Next, we investigated whether NO release from JGPN neurons was responsible for the hyperpolarization observed in type I cells. To test this, we used several different approaches. First, we exposed isolated type I cell clusters, grown in the absence of GPN neurons, to the NO donor SNP (500 μM). As exemplified in Figure 11*A*, SNP mimicked the ATP-induced hyperpolarization of the type I cell observed in cocultures. For a group of nine cells, SNP hyperpolarized the membrane potential from a mean resting level of -47.3 ± 4.8 to -53.2 ± 6.2 mV; the mean ± SEM change (ΔV_m) in membrane potential induced by 500 μM SNP is summarized in Figure 11*C* ($n = 9$). Second, we exposed cocultures to the NO scavenger cPTIO (Summers et al., 1999). As illustrated in Figure 11*B*, preincubation (>2 min) with 500–1000 μM cPTIO abolished irreversibly the ATP-induced hyperpolarization in cocultured type I cells. The time-dependent decrease in magnitude of the ATP-induced hyperpolarization in the presence of cPTIO is illustrated for several different coculture preparations in Figure 11*C* ($n = 6$; data represent mean ± SEM). Third, to further support the involvement of NO in the ATP-induced hyperpolarization in JGPN neurons, we exposed cocultures to the neuronal NOS inhibitor L-NAME (500 μM), which also inhibited the observed hyperpolarization ($n = 3$) (supplemental Fig. 2, available at www.jneurosci.org as supplemental material). These data suggest that activation of P2X receptors on GPN soma/terminals could lead to NO release, which in turn initiates efferent inhibition of type I cell function via membrane hyperpolarization.

In the intact carotid body, basal NO release is thought to exert a tonic efferent inhibition of chemoreceptor function even under normoxic conditions (Prabhakar, 1999). This raises the possibility that, in cocultures of JGPN and type I clusters, basal NO release might blunt the hypoxic response in type I cells, and this effect might even be exaggerated because GPN neurons can also be directly excited by hypoxia, leading to voltage-dependent Ca^{2+} entry and possibly NO release (Campanucci et al., 2003; Campanucci and Nurse, 2005) (Fig. 1*A*). As exemplified in Figure 12*A*, hypoxia (PO_2 of ~5 mmHg) induced membrane depolarization (or a receptor potential) in type 1 cells cultured without neurons, and this response was unaffected by the NO scavenger cPTIO, as expected because the source of NO production (i.e., GPN neurons) was absent. For a group of six cells from different cultures, the mean hypoxia-induced depolarization was 7.5 ± 0.9

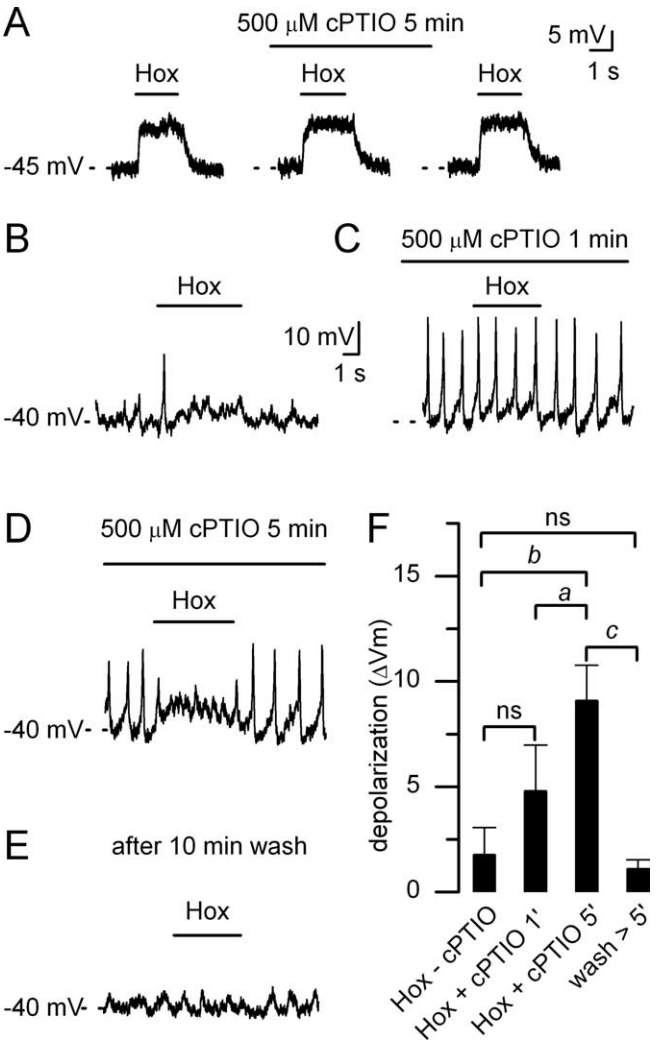

Figure 12. Effects of hypoxia on membrane potential of type I cells cocultured with JGPN neurons. ***A***, Representative example showing the lack of effect of cPTIO on the hypoxia (Hox)-induced depolarization (i.e., receptor potential) in type I cells cultured in the absence of GPN neurons. ***B***, Perfusion with a hypoxic solution (PO_2 of ~5 mmHg) caused a mild depolarization and spike generation in a type I cell that was part of a cell cluster grown in the presence of nearby JGPN neurons. ***C***, After 1 min incubation of the coculture with the NO scavenger cPTIO (500 μM), there was an increase in basal spontaneous spike activity of the type I cell. ***D***, After 5 min incubation with cPTIO, there was a potentiation of the original response to hypoxia (see ***A***). ***E***, All of these effects were fully reversible after washout of the drug for 10 min. ***F***, Histogram compares the time-dependent effect of cPTIO on the hypoxia-induced depolarization in a group ($n = 5$) of similar cocultured type I cells. Data are presented as mean ± SEM. $^{a}p < 0.05$; $^{b}p < 0.01$; $^{c}p < 0.001$.

and 7.3 ± 0.7 mV in the absence and presence of cPTIO, respectively ($p > 0.05$; $n = 6$). In cocultures, however, hypoxia was either ineffective ($n = 8$) or produced small (<2 mV) depolarizations ($n = 3$) in type I cells adjacent to GPN neurons. To test whether endogenous NO was active in the latter conditions, cocultures were exposed to 500 μM cPTIO for up to 8 min, and, interestingly, there was a gradual potentiation of the hypoxic response ($n = 5$). Data from a typical example are summarized in Figure 12*B–E* in which, after a weak initial hypoxic response in a type I cell (Fig. 12*B*), addition of 500 μM cPTIO caused an increase in basal spontaneous spike activity by 1 min exposure (Fig. 12*C*). At this stage, a hypoxia-induced depolarization was still detectable, but its magnitude progressively increased and was pronounced by 5 min exposure to 500 μM cPTIO (Fig. 12*D*). These effects were fully reversible after washout of cPTIO (Fig. 12*E*). Data from five similar experiments from different cocultures are summarized in Figure 12*F*. Together, these results strongly support a role of GPN neurons and/or their terminals in NO-mediated tonic inhibition of chemoreceptor cell function and in the blunting of the receptor response to hypoxia.

Paraganglia staining

During hypoxia, potential sources of ATP that could stimulate P2X receptors on GPN neurons or their processes include ATP released from CB type I cells (Zhang et al., 2000) and from red blood cells in the circulation (Ellsworth, 2000). To confirm that the microenvironment around GPN neurons *in situ* has ready access even to large molecules in the circulation, we fixed and perfused rat pups with a physiological salt solution containing Evans blue dye (McDonald and Blewett, 1981). This procedure revealed the anatomical structure of blood vessels surrounding the area in which both populations of GPN neurons were concentrated ($n = 4$) (supplemental Fig. 3*A*,*B*, available at www.jneurosci.org as supplemental material). As described previously (McDonald and Blewett, 1981), these groups of neurons, or paraganglia, are closely related to tortuous blood vessels that seem to spiral around the area surrounding the GPN neurons (supplemental Fig. 3*C*, available at www.jneurosci.org as supplemental material). Deposits of Evans blue dye were observed at these locations (supplemental Fig. 3*C*, available at www.jneurosci.org as supplemental material), confirming the high permeability of these blood vessels to the dye. These data suggest that GPN paraganglia may have direct access to substances released into the blood stream, for example ATP, released from red blood cells during hypoxia (for review, see Ellsworth, 2000).

Discussion

Expression of multiple P2X receptors in GPN neurons

In this study, we characterized purinergic responses in nNOS-positive autonomic neurons that are embedded in the rat GPN and are proposed to mediate efferent inhibition of CB chemoreceptors via release of NO (Prabhakar et al., 1993; Wang et al., 1993, 1995a;b; Grimes et al., 1994; Höhler et al., 1994). These GPN neurons were shown previously to be hypoxia sensitive and are distributed in two distinct populations, i.e., a proximal one near the branch point of the GPN and CSN and a more distal one located farther along the GPN (Campanucci et al., 2003; Campanucci and Nurse, 2005). Our present findings indicate that both populations of GPN neurons express a variety of purinergic P2X receptors, and, additionally, we demonstrate in a novel coculture preparation that activation of these receptors by ATP could indeed lead to NO-mediated inhibition of CB chemoreceptors.

The ATP-evoked responses appeared to involve multiple P2X receptors. Electrophysiological and pharmacological data were consistent with the *in situ* immunolocalization studies showing the presence of purinergic $P2X_2$, $P2X_3$, $P2X_4$, and $P2X_7$ subunits in GPN neurons. Additionally, the RT-PCR approach using tissue containing the distal population of GPN neurons detected not only the full-length $P2X_2$ isoform but also a splice variant, $P2X_{2(b)}$, which contains a 207 bp deletion in the C-terminal domain and is expressed in other autonomic neurons (Simon et al., 1997; Schädlich et al., 2001). This variant desensitizes more rapidly (approximately fivefold faster) during prolonged ATP application than the longer $P2X_2$ isoform (Simon et al., 1997). The combined data suggested functional expression of at least heteromeric $P2X_2$–$P2X_3$, homomeric $P2X_4$, and homomeric $P2X_7$ re-

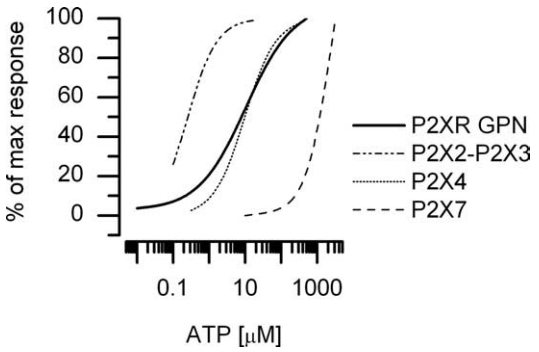

Figure 13. Fitted curves for the dose–response relationship for ATP at P2X receptors expressed in GPN neurons compared with heterologously expressed $P2X_2$–$P2X_3$ heteromultimeric receptors (Lewis et al., 1995) and $P2X_4$ (Bo et al., 1995) and $P2X_7$ (Chessell et al., 1998) homomultimeric receptors. The solid curve for native receptors in GPN neurons reflects a combination of the properties of the other receptors.

ceptors. The occurrence of heteromeric $P2X_2$–$P2X_3$ receptors was inferred from the observation that application of the ATP agonist α,β-MeATP activated inward currents with slow desensitization kinetics (Lewis et al., 1995; Radford et al., 1997) (for review, see Ralevic and Burnstock, 1998). These data, however, do not rule out the possibility that homomeric $P2X_2$ and homomeric $P2X_3$ receptors are also present.

Several pharmacological approaches indicated functional expression of $P2X_7$ receptors in GPN neurons. Consistent with our electrophysiological data, $P2X_7$ purinergic subunits were immunolocalized in both populations of GPN neurons in culture. Although $P2X_7$ subunits were localized in the soma of proximal GPN neurons *in situ*, they were not detectable on the soma of the distal population, which appeared to be contacted by $P2X_7$-immunopositive nerve endings. This raises the possibility that local circuits involving purinergic transmission may provide a means of cell-to-cell communication among GPN neurons and that $P2X_7$ subunits are targeted to nerve endings as evidenced by the distribution of $P2X_7$ immunostaining of isolated distal GPN neurons before and after process formation in culture. In this regard, it has been reported that $P2X_7$ receptors are targeted to presynaptic terminals in both the CNS and PNS (Deuchars et al., 2001).

Our electrophysiological, immunofluorescence, and RT-PCR studies also uncovered a role for $P2X_4$ receptors. In particular, IVM, a homomeric $P2X_4$ potentiator (Khakh et al., 1999), enhanced ATP-evoked currents in ~38% of the neurons, and this effect was likely mediated by $P2X_4$ receptors. Surprisingly, our immunofluorescence data indicated that almost all GPN neurons were positive for $P2X_4$ immunoreactivity. The reasons for this discrepancy are unknown, although $P2X_4$ subunits may form a heteromultimeric variant with a different pharmacological profile than the homomeric form. Indeed, $P2X_4$–$P2X_6$ heteromeric receptors are potentiated by IVM (Khakh et al., 1999), but this does not explain the inhibition of the ATP-evoked response by IVM in ~38% of the cells. An inhibitory effect of IVM has been reported in other native neuronal tissues, although the mechanisms are not understood (De Roo et al., 2003).

A comparison of fitted curves for the ATP dose–response curves for P2X receptors expressed in GPN neurons and for heterologously expressed $P2X_2$–$P2X_3$ heteromultimers (Lewis et al., 1995), homomeric $P2X_4$ (Bo et al., 1995), and homomeric $P2X_7$ (Chessell et al., 1998) receptors is shown in Figure 13. The EC_{50} for ATP on GPN neurons was close to that for $P2X_4$ receptors, but the dose–response curve deviated from the $P2X_4$ profile at lower and higher ATP concentrations (Fig. 13). The deviation is consistent with the additional presence of $P2X_2$–$P2X_3$ and $P2X_7$ receptors, which should allow GPN neurons to be activated over a broad range of ATP concentrations given that $P2X_2$–$P2X_3$ heteromultimers possess an EC_{50} of ~1 μM, whereas $P2X_4$ and $P2X_7$ homomeric receptors possess EC_{50} values of 10 and $\geq$100 μM, respectively.

Role of GPN neurons in carotid body chemoreceptor inhibition

In our immunofluorescence studies *in situ*, nNOS- and $P2X_7$-positive nerve fibers, which appeared to originate from GPN neurons, were found in close proximity to CB chemoreceptor cells. These $P2X_7$-positive fibers were also immunopositive for $P2X_3$ subunits, suggesting that the terminal branches of GPN neurons may also express multiple P2X receptors similar to the soma. Although we did observe $P2X_7$-positive immunoreactivity associated with blood vessels in the rat CB (Fig. 8*H*), this labeling did not colocalize with neuronal markers (Fig. 8*G–I*) and was likely attributable to the known expression of $P2X_7$ subunits in smooth muscle and endothelium of blood vessels (for review, see Burnstock, 2002). To investigate directly whether P2X signaling might play a role in efferent CB chemoreceptor (type I cell) inhibition, we developed a novel coculture preparation consisting of type I cell clusters and juxtaposed GPN neurons. Interestingly, activation of P2X receptors on cocultured neurons by ATP or BzATP caused type I cell hyperpolarization that was prevented by preincubation with the NO scavenger cPTIO and mimicked by application of the NO donor SNP to type I cells cultured alone. These data suggest that NO was the "inhibitory signal" released on purinergic activation of cocultured GPN neurons. Additionally, the hypoxia-induced receptor potential recorded in type I cells was suppressed in similar cocultures, and this was apparently attributable to the release of NO from GPN neurons because it could be reversed by cPTIO. Because GPN neurons are also excited by hypoxia (Campanucci et al., 2003; Campanucci and Nurse, 2005), this stimulus may also lead to voltage-gated Ca^{2+} entry, NOS activation, and NO-mediated inhibition of the receptor potential in type I cells (Prabhakar, 1999). Additional interactions may occur between hypoxia and ATP in light of a recent report indicating an inhibitory effect of ATP, acting via P2Y receptors, on the hypoxia-induced $[Ca^{2+}]_i$ elevation in isolated adult rat type I cells (Xu et al., 2005).

A physiological model for the activation of GPN neurons

Our findings have led to a "working model" for the role of GPN neurons in the efferent inhibition of the rat CB via their activation by hypoxia and ATP. As summarized in supplemental Figure 1 (available at www.jneurosci.org as supplemental material), a reduction in blood PO_2 (hypoxemia) causes at least four effects, as follows: (1) Inhibition of background [TASK-1 (TWIK-related acid-sensitive K^+ channels)-like] K^+ and large-conductance Ca^{2+} activated K^+ channels in carotid body type I cells (for review, see López-Barneo et al., 2001), leading to or enhancing membrane depolarization, activation of L-type Ca^{2+} channels, and neurotransmitter (ATP and ACh) release (Zhang et al., 2000). These neurotransmitters act on petrosal sensory nerve endings via $P2X_2$–$P2X_3$ receptors (Prasad et al., 2001; Rong et al., 2003) and nicotinic ACh receptors, leading to a compensatory reflex increase in ventilation and restoration of blood PO_2. (2) ATP, released from type I cells during hypoxia, may act on nearby GPN nerve terminals, which express multiple P2X receptors con-

taining $P2X_2$, $P2X_{2(b)}$, $P2X_3$, $P2X_4$, and $P2X_7$ subunits. Activation of these P2X receptors causes Ca^{2+} influx and nNOS activation, leading to NO synthesis and release. NO actions on type I cells lead to inhibition of neurotransmitter release via membrane hyperpolarization (Silva and Lewis, 2002; this study) and/or direct inhibition of L-type Ca^{2+} channels (Summers et al., 1999). (3) Hypoxia causes red blood cells to release ATP (for review, see Ellsworth, 2000), which may directly stimulate GPN neurons via P2X receptors and endothelial cells via P2Y receptors (Ellsworth, 2000). Indeed, staining of whole mount of the GPN during perfusion with the large-molecular-weight Evans blue dye (supplemental Fig. 3, available at www.jneurosci.org as supplemental material) confirmed that GPN neurons were associated with an intricate network of fenestrated capillaries (McDonald and Blewett, 1981), thereby providing easy access to blood-borne substances such as ATP, present in millimolar quantities in erythrocytes (Miseta et al., 1993). (4) Hypoxia may also activate GPN neurons by inhibiting background K^+ channels (Campanucci et al., 2003), leading to increased firing, voltage-gated Ca^{2+} entry, nNOS activation, and NO release. Thus, activation of GPN neurons by hypoxia and/or ATP, released during hypoxic stress, would lead to efferent inhibition of CB chemoreceptors, thereby providing a dual mechanism for negative feedback control of respiration via the same neuronal pathway.

References

Bianchi BR, Lynch KJ, Touma E, Niforatos W, Burgard EC, Alexander KM, Park HS, Yu H, Metzger R, Kowaluk E, Jarvis MF, van Biesen T (1999) Pharmacological characterization of recombinant human and rat P2X receptor subtypes. Eur J Pharmacol 376:127–138.

Bo X, Zhang Y, Nassar M, Burnstock G, Schoepfer R (1995) A P2X purinoceptor cDNA conferring a novel pharmacological profile. FEBS Lett 375:129–133.

Brake AJ, Wagenbach MJ, Julius D (1994) New structural motif for ligand-gated ion channels defined by an ionotropic ATP receptor. Nature 371:519–523.

Burnstock G (2002) Purinergic signaling and vascular cell proliferation and death. Arterioscler Thromb Vasc Biol 22:364–373.

Buttigieg J, Nurse CA (2004) Detection of hypoxia-evoked ATP release from chemoreceptor cells of the rat carotid body. Biochem Biophys Res Commun 322:82–87.

Campanucci VA, Nurse CA (2005) Biophysical characterization of whole-cell currents in O_2-sensitive neurons from the rat glossopharyngeal nerve. Neuroscience 132:437–451.

Campanucci VA, Fearon IM, Nurse CA (2003) A novel O_2-sensing mechanism in rat glossopharyngeal neurones mediated by a halothane-inhibitable background K^+ conductance. J Physiol (Lond) 548:731–743.

Chessell IP, Simon J, Hibell AD, Michel AD, Barnard EA, Humphrey PP (1998) Cloning and functional characterisation of the mouse P2X7 receptor. FEBS Lett 439:26–30.

De Roo M, Rodeau JL, Schlichter R (2003) Dehydroepiandrosterone potentiates native ionotropic ATP receptors containing the P2X2 subunit in rat sensory neurones. J Physiol (Lond) 552:59–71.

Deuchars SA, Atkinson L, Brooke RE, Musa H, Milligan CJ, Batten TF, Buckley NJ, Parson SH, Deuchars J (2001) Neuronal $P2X_7$ receptors are targeted to presynaptic terminals in the central and peripheral nervous systems. J Neurosci 21:7143–7152.

Dunn PM, Zhong Y, Burnstock G (2001) P2X receptors in peripheral neurons. Prog Neurobiol 65:107–134.

Ellsworth ML (2000) The red blood cell as an oxygen sensor: what is the evidence? Acta Physiol Scand 168:551–559.

Evans RJ, Lewis C, Virginio C, Lundstrom K, Buell G, Surprenant A, North RA (1996) Ionic permeability of, and divalent cation effects on, two ATP-gated cation channels (P2X receptors) expressed in mammalian cells. J Physiol (Lond) 497:413–422.

Fung ML, Ye JS, Fung PC (2001) Acute hypoxia elevates nitric oxide generation in rat carotid body in vitro. Pflügers Arch 442:903–909.

Giegerich R, Meyer F, Schleiermacher C (1996) GeneFisher: software support for the detection of postulated genes. Proc Int Conf Intell Syst Mol Biol 4:68–77.

Gonzalez C, Almaraz L, Obeso A, Rigual R (1994) Carotid body chemoreceptors: from natural stimuli to sensory discharges. Physiol Rev 74:829–898.

Grimes PA, Lahiri S, Stone R, Mokashi A, Chug D (1994) Nitric oxide synthase occurs in neurons and nerve fibers of the carotid body. Adv Exp Med Biol 360:221–224.

He L, Chen J, Dinger B, Stensaas L, Fidone S (2006) Effect of chronic hypoxia on purinergic synaptic transmission in rat carotid body. J Appl Physiol 100:157–162.

Höhler B, Mayer B, Kummer W (1994) Nitric oxide synthase in the rat carotid body and carotid sinus. Cell Tissue Res 276:559–564.

Jiang LH, Mackenzie AB, North RA, Surprenant A (2000) Brilliant blue G selectively blocks ATP-gated rat $P2X_7$ receptors. Mol Pharmacol 58:82–88.

Khakh BS (2001) Molecular physiology of P2X receptors and ATP signalling at synapses. Nat Rev Neurosci 2:165–174.

Khakh BS, Proctor WR, Dunwiddie TV, Labarca C, Lester HA (1999) Allosteric control of gating and kinetics at $P2X_4$ receptor channels. J Neurosci 19:7289–7299.

Khakh BS, Burnstock G, Kennedy C, King BF, North RA, Seguela P, Voigt M, Humphrey PP (2001) International union of pharmacology. XXIV. Current status of the nomenclature and properties of P2X receptors and their subunits. Pharmacol Rev 53:107–118.

Kline DD, Yang T, Huang PL, Prabhakar NR (1998) Altered respiratory responses to hypoxia in mutant mice deficient in neuronal nitric oxide synthase. J Physiol (Lond) 511:273–287.

Lewis C, Neidhart S, Holy C, North RA, Buell G, Surprenant A (1995) Coexpression of P2X2 and P2X3 receptor subunits can account for ATP-gated currents in sensory neurons. Nature 377:432–435.

López-Barneo J, Pardal R, Ortega-Sáenz P (2001) Cellular mechanism of oxygen sensing. Annu Rev Physiol 63:259–287.

McDonald DM, Blewett RW (1981) Location and size of carotid body-like organs (paraganglia) revealed in rats by the permeability of blood vessels to Evans blue dye. J Neurocytol 10:607–643.

Miseta A, Bogner P, Berenyi E, Kellermayer M, Galambos C, Wheatley DN, Cameron IL (1993) Relationship between cellular ATP, potassium, sodium and magnesium concentrations in mammalian and avian erythrocytes. Biochim Biophys Acta 1175:133–139.

Murgia M, Hanau S, Pizzo P, Rippa M, Di Virgilio F (1993) Oxidized ATP. An irreversible inhibitor of the macrophage purinergic P2Z receptor. J Biol Chem 268:8199–8203.

North RA (2002) Molecular physiology of P2X receptors. Physiol Rev 82:1013–1067.

North RA, Surprenant A (2000) Pharmacology of cloned P2X receptors. Annu Rev Pharmacol Toxicol 40:563–580.

Nurse CA (2005) Neurotransmission and neuromodulation in the chemosensory carotid body. Auton Neurosci 120:1–9.

Nurse CA, Zhang M (1999) Acetylcholine contributes to hypoxic chemotransmission in co-cultures of rat type 1 cells and petrosal neurons. Respir Physiol 115:189–199.

Prabhakar NR (1999) NO and CO as second messengers in oxygen sensing in the carotid body. Respir Physiol 115:161–168.

Prabhakar NR, Kumar GK, Chang CH, Agani FH, Haxhiu MA (1993) Nitric oxide in sensory function of the carotid body. Brain Res 625:16–22.

Prasad M, Fearon IM, Zhang M, Laing M, Vollmer C, Nurse CA (2001) Expression of P2X2 and P2X3 receptor subunits in rat carotid body afferent neurones: role in chemosensory signalling. J Physiol (Lond) 537:667–677.

Radford KM, Virginio C, Surprenant A, North RA, Kawashima E (1997) Baculovirus expression provides direct evidence for heteromeric assembly of $P2X_2$ and $P2X_3$ receptors. J Neurosci 17:6529–6533.

Ralevic V, Burnstock G (1998) Receptors for purines and pyrimidines. Pharmacol Rev 50:413–492.

Rong W, Gourine AV, Cockayne DA, Xiang Z, Ford AP, Spyer KM, Burnstock G (2003) Pivotal role of nucleotide $P2X_2$ receptor subunit of the ATP-gated ion channel mediating ventilatory responses to hypoxia. J Neurosci 23:11315–11321.

Schädlich H, Wirkner K, Franke H, Bauer S, Grosche J, Burnstock G, Reichen-

bach A, Illes P, Allgaier C (2001) $P2X_2$, $P2X_{2-2}$ and $P2X_5$ receptor subunit expression and function in rat thoracolumbar sympathetic neurons. J Neurochem 79:997–1003.

Silva JM, Lewis DL (2002) Nitric oxide enhances Ca^{2+}-dependent K^+ channel activity in rat carotid body cells. Pflügers Arch 443:671–675.

Simon J, Kidd EJ, Smith FM, Chessell IP, Murrell-Lagnado R, Humphrey PP, Barnard EA (1997) Localization and functional expression of splice variants of the P2X2 receptor. Mol Pharmacol 52:237–248.

Summers BA, Overholt JL, Prabhakar NR (1999) Nitric oxide inhibits L-type Ca^{2+} current in glomus cells of the rabbit carotid body via a cGMP-independent mechanism. J Neurophysiol 81:1449–1457.

Vincent SR (1994) Nitric oxide: a radical neurotransmitter in the central nervous system. Prog Neurobiol 42:129–160.

Wang ZZ, Bredt DS, Fidone SJ, Stensaas LJ (1993) Neurons synthesizing nitric oxide innervate the mammalian carotid body. J Comp Neurol 336:419–432.

Wang ZZ, Stensaas LJ, Bredt DS, Dinger B, Fidone SJ (1994) Localization and actions of nitric oxide in the cat carotid body. Neuroscience 60:275–286.

Wang ZZ, Dinger BG, Stensaas LJ, Fidone SJ (1995a) The role of nitric oxide in carotid chemoreception. Biol Signals 4:109–116.

Wang ZZ, Stensaas LJ, Dinger BG, Fidone SJ (1995b) Nitric oxide mediates chemoreceptor inhibition in the cat carotid body. Neuroscience 65:217–229.

Xu J, Xu F, Tse FW, Tse A (2005) ATP inhibits the hypoxia response in type I cells of rat carotid bodies. J Neurochem 92:1419–1430.

Zhang M, Nurse CA (2000) Does endogenous 5-HT mediate spontaneous rhythmic activity in chemoreceptor clusters of rat carotid body? Brain Res 872:199–203.

Zhang M, Nurse CA (2004) CO_2/pH chemosensory signalling in co-cultures of rat carotid body receptors and petrosal neurons: role of ATP and ACh. J Neurophysiol 92:3433–3445.

Zhang M, Zhong H, Vollmer C, Nurse CA (2000) Co-release of ATP and ACh mediates hypoxic signalling at rat carotid body chemoreceptors. J Physiol (Lond) 525:143–158.

Zhong H, Zhang M, Nurse CA (1997) Synapse formation and hypoxic signalling in co-cultures of rat petrosal neurones and carotid body type 1 cells. J Physiol (Lond) 503:599–612.